

Highly uniform GaSb quantum dots with indirect-direct bandgap cross-over at telecom range

*Abhiroop Chellu, Joonas Hilska, Jussi-Pekka Penttinen, Teemu Hakkarainen**

Optoelectronics Research Centre, Physics Unit, Tampere University, Korkeakoulunkatu 3, 33720 Tampere, Finland.

KEYWORDS Quantum dots, Nanostructures, Nanoholes, Droplets, GaSb, Photoluminescence

ABSTRACT

We demonstrate a new semiconductor quantum system based on GaSb quantum dots (QDs) embedded in single-crystalline AlGaSb matrix by filling droplet-etched nanoholes. The droplet-mediated growth mechanism allows formation of low QD densities required for non-classical single-QD light sources. The photoluminescence (PL) experiments reveal that the GaSb QDs have an indirect-direct bandgap cross-over at telecom wavelengths. This is due to the alignment of the Γ and L valleys in the conduction band as a result of quantum confinement controlled by dimensions of the nanostructure. We show that in the direct bandgap regime close to 1.5 μm wavelength, the GaSb QDs have a type I band alignment and exhibit excitonic emission with narrow spectral lines and very low inhomogeneous broadening of PL emission owing to the high material quality and dimensional uniformity. These properties are extremely promising in terms of applications in infrared quantum optics and quantum photonic integration.

Semiconductor quantum dots (QD) embedded in a single-crystalline host matrix are important building blocks of emerging quantum technologies based on non-classical light sources, such as single- or entangled-photon emitters [1,2]. Such quantum nanostructures can be fabricated by several techniques including Stranski-Krastanov (SK) growth [3,4], droplet epitaxy [5-7], growth inside pyramidal holes [8], vapor-liquid-solid growth in nanowires [9], and filling of nanoholes formed by local droplet etching (LDE) [10]. The approach based on filling nanoholes is particularly interesting due to its advantages which include narrow exciton linewidths [11], extremely small inhomogeneous broadening due to size uniformity [12], bright single-photon emission [13], and vanishing fine structure splitting owing to the dimensional symmetry and lack of strain-induced piezoelectric asymmetries [14]. These properties have enabled the use of GaAs/AlGaAs QDs grown by filling nanoholes in non-classical light sources providing state-of-the-art performance in terms of photon indistinguishability and entanglement [13,15,16]. However, the operation of the light sources based on this approach is restricted to the 680-780 nm spectral range [11] due to the limited direct bandgap range of (Al)GaAs alloys.

The reports on local droplet etching (LDE) of nanoholes were limited to the (Al)GaAs alloy system [10,17-24] until recently when we demonstrated highly controllable LDE of AlGaSb with Ga droplets [25]. In contrast to the LDE of arsenides, the low vapor pressure of Sb allows deterministic control of the group V beam pressure which essentially controls nanohole etching process by adjusting the Sb source needle valve. Furthermore, the GaSb-based materials provide suitable bandgaps for accessing the technologically important telecom wavelengths [26] and even beyond that to the mid-infrared wavelength range [27] with compatibility for silicon photonic integration [28]. The additional benefits of the AlGa(As)Sb alloys include a very high refractive index contrast [29] (exceeding that of AlGaAs), which is important for constructing photonic

devices. Moreover, the lattice mismatch between GaSb-based materials and dissimilar substrates can be relaxed right at the first interface by formation of a network of 90°-dislocations [30,31] and exploitation of nucleation layers [32], which is particularly useful considering direct growth of QD emitters on silicon waveguides for chip-level quantum photonic integration.

Here, we report a new quantum system based on GaSb QDs in AlGaSb matrix formed by filling droplet-etched nanoholes. We use the same methodology as in our previous work for nanohole etching [25] with the exception that Al droplets are used instead of Ga in order to avoid charge carrier confinement in the ring structure formed around the nanoholes in the LDE process. Optically active and highly uniform QDs are then formed by depositing a thin GaSb quantum well (QW) on the droplet-etched surface, similarly to the GaAs/AlGaAs system [10]. The resulting QDs exhibit excitonic emission at telecom wavelengths with type I band alignment contrary to the existing antimonide QDs such as InSb/InAs [33], InSb/GaAs, and GaSb/GaAs QDs [34,35], which confine only holes while the electrons are bound outside the QD.

Formation of GaSb QDs in an AlGaSb matrix begins with etching of nanoholes in AlGaSb surfaces with Al droplets. Figure 1 shows atomic force microscopy (AFM) images of the AlGaSb surfaces after droplet etching at 500°C and 395°C with Al droplets formed by deposition of different Al coverages θ_{Al} . As shown in Fig. 1(a), LDE at 500°C with $\theta_{Al}=3.2$ monolayers (ML) results in mobile droplets and inhomogeneous nanoholes. For $\theta_{Al}=2.0$ ML, we observed well defined nanoholes, but their size distribution is bimodal, as shown in Fig. 1(b). Similar morphologies have been observed in AlGaAs surfaces after LDE with Al droplets due to a change in surface reconstruction at high Al coverages [36,37]. For θ_{Al} ranging from 1.5 to 1.25 ML we observe a monomodal distribution of uniform nanoholes. No nanoholes are observed for $\theta_{Al}=1.15$ ML (See Fig. S1 in the Supp. Info), indicating that the critical thickness for Al droplet formation

on AlGaSb is approximately 1.2 ML which is consistent with our findings on Ga droplet formation on the same surface [25], as well as with the group III metal coverage required for saturating the (1x3) surface reconstruction [38]. In case of LDE at 395°C, a bimodal nanohole distribution with additional mobile droplets is observed for $\theta_{Al}=2.0$ ML (Fig. 1(e)). A monomodal distribution of uniform nanoholes is again recovered by reducing θ_{Al} down to 1.5 ML. The densities of the uniform nanoholes formed at 500°C and 395°C are $1.9 \times 10^6 \text{ cm}^{-2}$ and $2.6 \times 10^7 \text{ cm}^{-2}$, which both are low enough to allow addressing individual QDs in optical experiments. According to the cross-sectional profiles shown in Fig. 1(g) and (f), the nanohole formed at 500°C with $\theta_{Al}=1.5$ ML is 70 nm deep, while the hole formed at 395°C with the same coverage is around 12 nm deep. This reduction in hole depth is a result of the droplets becoming smaller and denser as the temperature is decreased. At the same time, the lateral dimensions of the hole also decreases as the temperature is reduced. The slope of the hole sidewalls is around 55° which matches with the (111) crystal planes.

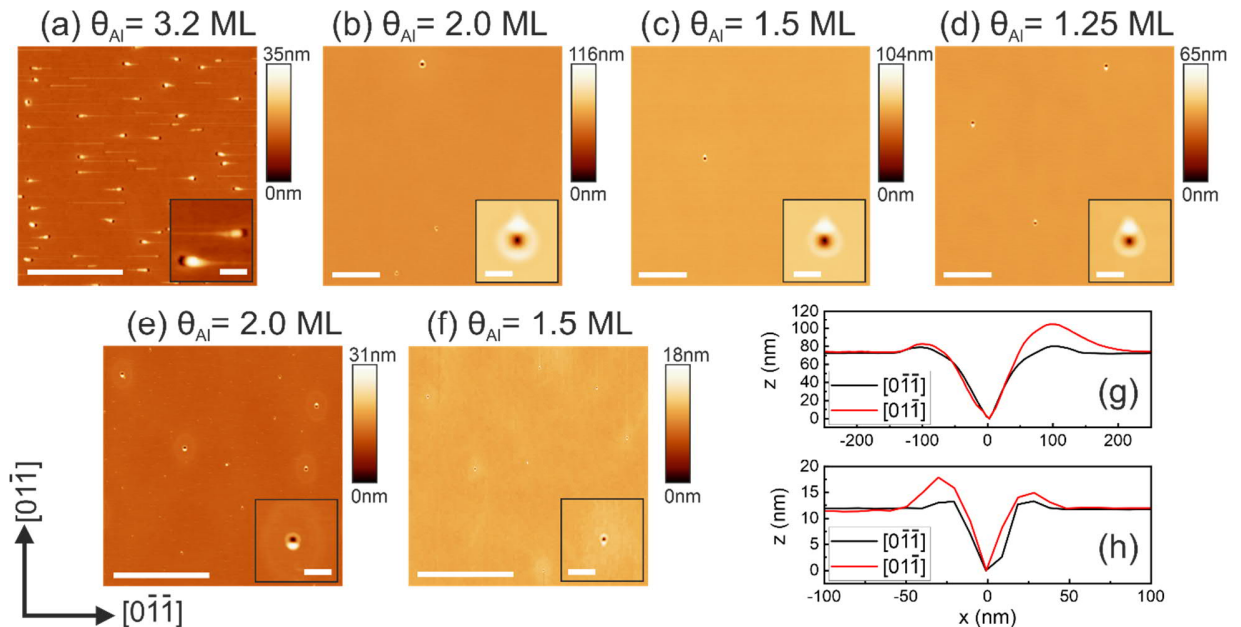


Figure 1. AFM images of the AlGaSb surface after nanohole etching with Al droplets. (a)-(d) show the holes formed at 500°C and (e)-(f) at 395°C by deposition of different amounts of Al as measured by the monolayer coverage θ_{Al} . The cross-sectional profiles in (g) and (h) are taken from (c) and (f), respectively for both $[0\bar{1}1]$ and $[0\bar{1}\bar{1}]$ crystal directions. The scale bars are 2 μm in the main images and 200 nm in the insets in (a)-(f).

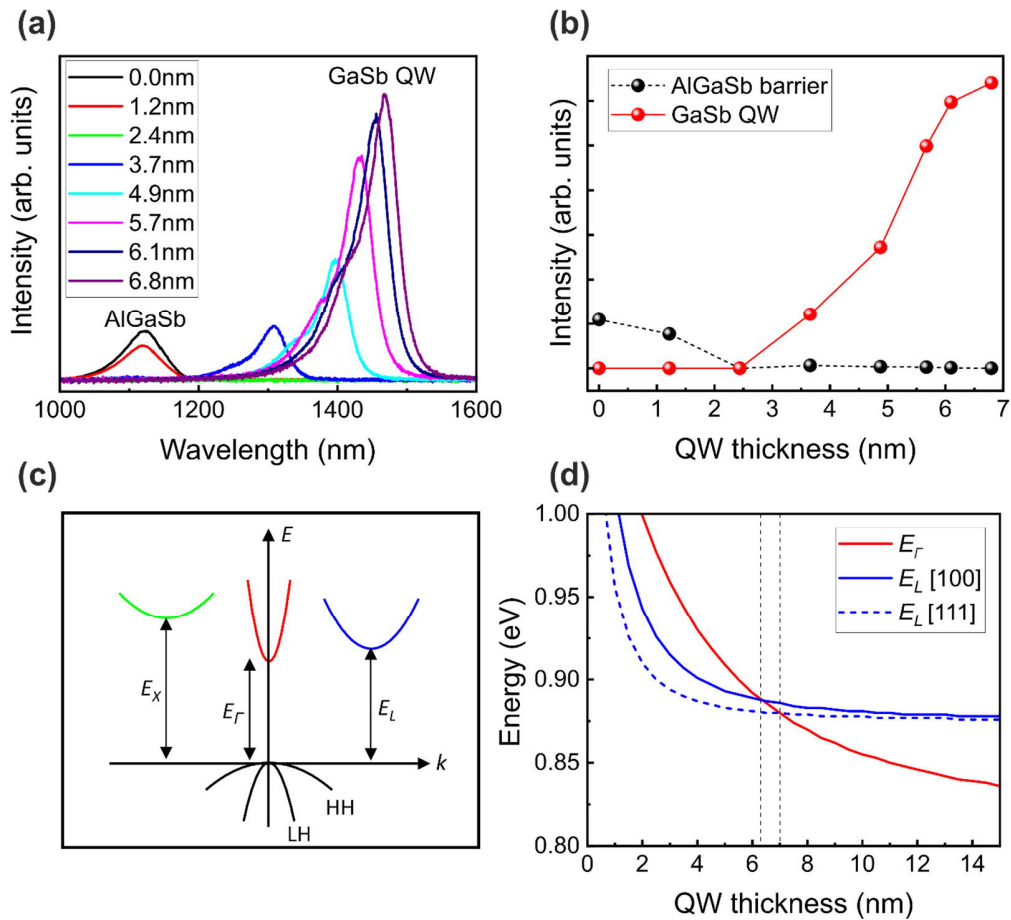


Figure 2. (a) Room temperature PL spectra showing the AlGaSb barrier and GaSb QW emission for different QW thicknesses. (b) The intensities of the peaks from (a) as a function of the QW thickness. (c) A simplified energy band diagram of GaSb bulk including heavy hole (HH) and light hole (LH) valence bands and Γ , L , and X valleys in the conduction band. (d) Energies of the lowest quantum confined electron states in Γ and L valleys as a function of QW thickness. The energies

are referenced with respect to the top of the valence band. The vertical dashed lines indicate the indirect-direct bandgap crossover for confinements in the [100] and [111] directions.

Optically active GaSb nanostructures are then formed by filling the 12 nm deep nanoholes shown in Fig. 1(f) by depositing GaSb QWs with different thicknesses and embedding them in AlGaSb. The room temperature PL of such structures is shown in Fig. 2. As shown in Fig. 2(a), for QW thicknesses of 0 nm and 1.2 nm, we observe the PL only from the AlGaSb matrix at around 1120 nm, while no PL emission at all is detected in case of 2.4 nm. For QW thicknesses from 3.7-6.8 nm we observe the GaSb QW peak which redshifts and intensifies as the QW thickness is increased, as summarized in Fig. 2(b). These results can be explained by looking at the GaSb bandstructure which is illustrated in Fig. 2(c). While GaSb in bulk form is a direct bandgap semiconductor with conduction band minimum at Γ point, the energy separation between the Γ and L points is relatively small. The electron effective mass at Γ is $m^*(\Gamma) = 0.039m_0$, where m_0 is the electron mass, while at the asymmetric L valley we have longitudinal and transversal components $m_l^*(L) = 1.3m_0$ and $m_t^*(L) = 0.1m_0$ [27]. Because of this significant difference in the effective masses, the quantum effect is more pronounced for the Γ electrons than for the L electrons which results in direct-indirect bandgap crossover as the dimensions of the nanostructure are reduced, as reported for GaSb/AlSb QWs [39]. In order to obtain a quantitative description for the cross-over, we solve the electron energy states in the GaSb/AlGaSb QW using the effective mass approach with finite barriers. For confinement in the [100] direction (the growth direction) we use a projected effective mass of $0.52m_0$ [39], while for the confinement in the [111] direction, the longitudinal mass $m_l^*(L)$ can be used. The band nonparabolicities are accounted as in [39] by corrections to the effective masses as $m_{NP}^*(\Gamma) = m^*(\Gamma) \left(1 + \frac{2.5 \text{ nm}}{t_{QW}}\right)$ for Γ and $m_{NP}^*(L) =$

$m^*(L) \left(1 + \frac{0.6 \text{ nm}}{t_{QW}}\right)$ for L , with t_{QW} being the QW thickness in nanometers. The solutions for the lowest electron states for Γ and L points are shown in Fig. 2(d), which confirms that the energy structure of the QW is indirect when its dimensions are small. In case of the [100] confinement, the crossover from indirect to direct bandgap is observed when the QW thickness is increased beyond 6.3 nm, which is consistent with the PL intensity trend shown in Fig. 2(b). In case of [111] confinement, the crossover is observed at slightly larger QW thickness due to the larger effective mass.

Similar trends in the GaSb QW PL peak intensity and position with increasing t_{QW} are observed also at 20 K (Fig. 3(a)). However, for QW thicknesses of 5.7 nm and 6.1 nm we observed additional narrow peaks P1-P3 which are not present in the reference QW grown on a planar AlGaSb surface without nanoholes, which suggest localized emission at the nanoholes. As revealed by the PL spectra obtained with different excitation power densities (Fig. 3(b)) and the power-dependency of the peak intensities (Fig. 3(c)), the P1 and P2 peaks exhibit a typical behavior of QD ground state and first excited state emission, respectively. The intensity I of the P1 peak exhibits a linear dependency of the PL intensity on the excitation power P , *i.e.* $I \sim P^{1.00}$, which is a sign of typical excitonic behavior at the ground state of the localized system. Peak P2, on the other hand, shows superlinear power-dependency with $I \sim P^{1.37}$ and emerges at higher excitation powers than P1 does, which is typical behavior of the first excited state [40]. The intensity of P2 also keeps increasing as a function of excitation power beyond the point of saturation of P1 as expected for the excited state emission. P3 shows a linear power-dependency and emerges at lower excitation powers than P2, which suggest that it is a ground state of another localized system rather than the second excited state of the QD inside the hole. A similar PL peak has been observed in case of GaAs/AlGaAs QDs grown by filling droplet-etched nanoholes and attributed to localized QW emission at the

edge of ring structure outside the nanohole [41]. Since the PL signal was collected from a large number of QDs, the width of the P1 peak below saturation level represents the inhomogeneous broadening as a result of QD size dispersion. As shown in the inset in Fig.3(b), the full-width-at-half-maximum (FWHM) for the P1 peak is just 8 meV, which indicates significantly smaller inhomogeneous broadening than in InAs SK QDs (typically tens of meV) [42] and even smaller than in GaAs/AlGaAs QDs formed by filling droplet etched nanoholes [10].

It should be noted that no QD emission is observed for QW thicknesses below 5.7 nm, and then from 5.7 nm to 6.1 nm we observe a red shift of the P1 peak from 1470 nm to 1478 nm similarly to the QW emission in the direct bandgap regime. This is due to the cross-over from indirect to direct bandgap as the size of the nanostructure increases, just like shown for the QW in Fig. 2. Since the QDs were formed by completely filling 12 nm deep nanoholes (See Fig. S2 in Supp. Info), the critical dimensions for the indirect-direct crossover appear to be larger for GaSb QDs than for GaSb QWs. The quantum effect can be expected to be larger in a zero-dimensional structure, but here, the nanohole morphology brings additional confinement specifically in the [111] directions for which the electrons in the L valley experience the large longitudinal effective mass of $1.3m_0$. In such case, the critical size required for the indirect-direct crossover is expected to be larger than for the confinement in the [100] direction as shown in Fig. 2(d).

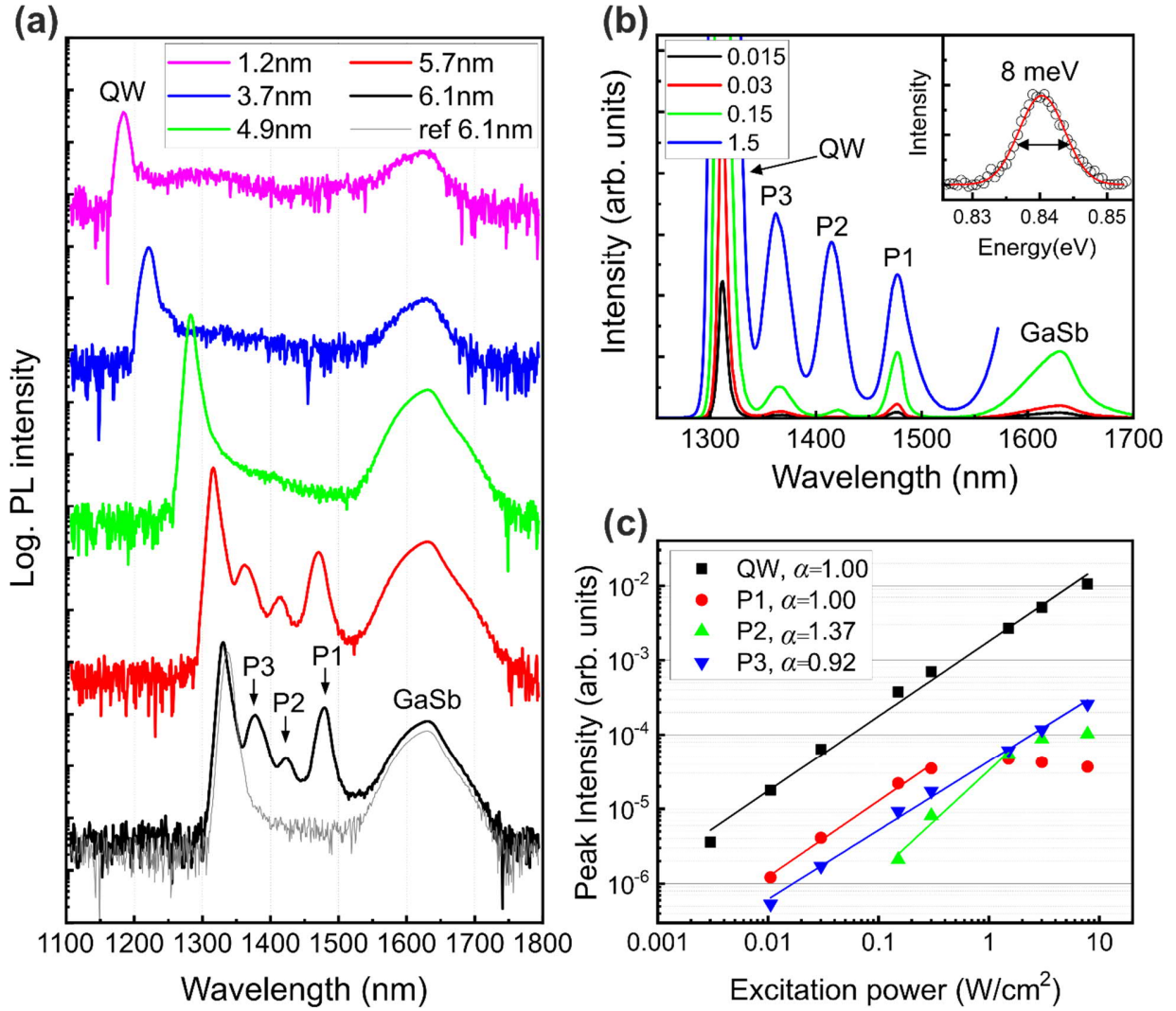


Figure 3. (a) PL spectra at 20 K showing the GaSb QW and GaSb bulk emission peaks as well as the QD peaks P1-P3 arising from emission in a large number of filled nanoholes. The reference spectrum presented by the gray line is measured from a 6.1 nm thick GaSb QW grown on a planar AlGaSb surface without nanoholes. (b) Excitation power-dependent spectra for the 5.7 nm sample, with laser power density indicated in W/cm^2 . The inset shows the P1 peak width for the lowest excitation power. The intensities (I) of the QW and QD peaks as a function of excitation power (P) are shown in (c). The solid lines represent fits with $I = A \times P^\alpha$, where A is a constant and α is the slope depending on the decay mechanism.

The luminescence properties of the GaSb/AlGaSb QDs formed by filling droplet-etched nanoholes were further investigated by single-QD PL spectroscopy. As shown in Fig. 4(a), they exhibit single-QD emission characterized by narrow emission lines. The excitation power-dependent measurement reveals a dominant single-exciton (X) peak with a slope of 1.1 (Fig. 4(b)). The width of the X line is 90 μeV , which is at the resolution limit of our optical setup. These results prove that the GaSb/AlGaSb QDs possess typical luminescence characteristics of excitonic recombination in a high-quality, 0-dimensional quantum system with type I band alignment. This is in contrast to other antimonide QDs, which have type II systems and thus exhibit broad emission peaks and blueshift of the exciton lines with increasing excitation power [43]. No biexciton emission is identified in the single-QD spectra. Instead, several peaks with a slope of <2 appear at lower energies when the excitation power is increased. These additional lines are most probably a collection of charged and neutral multi-excitonic lines as well as emission from other QDs. Such PL characteristics are typically observed for GaAs/AlGaAs QDs grown by filling droplet-etched nanoholes, with a clear biexciton emission being detectable using resonant excitation [15].

The PL observations clearly show the potential of the GaSb/AlGaSb QDs for non-classical light emission at infrared and telecom wavelengths, with wavelength tunability achievable by adjusting the QD dimensions. An additional benefit of the LDE-based QD formation mechanism is that the band structure of the QD material is widely tunable by alloying GaSb with other elements, such as As, In, and Bi. This provides the freedom to extend the emission wavelength to even longer wavelengths towards 2 μm and potentially beyond, and to simultaneously adjust the alignment of the Γ and L valleys in order to control the charge carrier recombination processes. Furthermore,

the indirect-direct bandgap cross-over could be utilized for triggering spontaneous emission in the QDs by interfacing them with piezoelectric strain elements or surface acoustic waves [44].

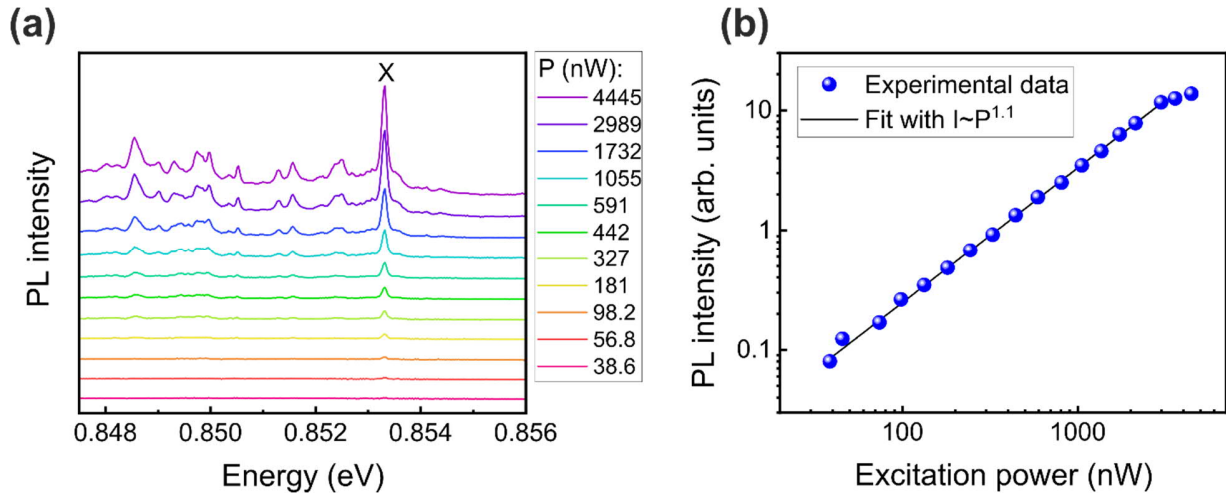


Figure 4. (a) Single-QD PL emission measured at 6 K with different excitation powers from the sample with 5.7 nm GaSb layer deposited on droplet-etched AlGaSb surface. The intensity of the single-exciton (X) peak is displayed in (b) as a function excitation power.

In conclusion, we have demonstrated a new type I semiconductor quantum system based on highly uniform GaSb QDs formed in AlGaSb matrix by filling droplet-etched nanoholes. This technique allows the formation of low QD densities required for single-QD quantum light sources. The GaSb QDs exhibit an indirect-direct bandgap cross-over at the telecom wavelength range, and thus allow access to a quantum system which can be tuned from highly luminescent to non-luminescent in a controllable way. In the direct bandgap regime at around 1.470 μm wavelength, the GaSb QDs exhibit excitonic emission narrow single exciton lines and very small inhomogeneous broadening which are extremely promising findings in terms of applications in infrared quantum optics and quantum photonic integration.

EXPERIMENTAL METHODS

Sample growth and layer structures

All samples were grown by solid-source molecular beam epitaxy (MBE) on n-GaSb(100) substrates. For the determination of nanohole density and morphology, we prepared samples following the procedure as described in [25]. Namely, after growth of 100 nm thick GaSb buffer and $\text{Al}_{0.3}\text{Ga}_{0.7}\text{Sb}$ layers at 500°C , the substrate was set to pyrometer temperatures between $395\text{--}500^\circ\text{C}$ for the droplet deposition and LDE steps. Al was deposited for different target coverages between $\theta_{\text{Al}}=1.15\text{--}3.2$ ML under a predetermined Sb-flux of 0.067 ML/s. The nanoholes were formed by letting the Al droplets react with the $\text{Al}_{0.3}\text{Ga}_{0.7}\text{Sb}$ surface under the same Sb-flux for 180 s, which was a long enough annealing time to ensure complete etching of the nanoholes and consumption of the liquid droplet.

For optical studies, the GaSb-filled nanoholes were grown on a 100 nm thick AlGaSb layer by following the same steps as above, with the GaSb QD filling performed immediately after the LDE step at the LDE temperature. After filling the nanoholes, the sample temperature was increased to 500°C while simultaneously capping the GaSb QDs with 100 nm of $\text{Al}_{0.3}\text{Ga}_{0.7}\text{Sb}$. To promote recombination in the QW/QD structure, the AlGaSb films were cladded on either side with 50 nm thick lattice-matched AlAsSb layers which confined the generated carriers to the AlGaSb matrix. Finally, to prevent oxidative degradation of the topmost AlAsSb layer under atmosphere, the structure was capped with 15 nm of GaSb. For all samples, the Ga and Al fluxes were 0.7 and 0.3 ML/s, respectively. The full layer structures are illustrated in Fig. S3 in the Supp. Info.

Photoluminescence spectroscopy

Room temperature PL spectra of the GaSb QWs were recorded using 532 nm excitation. The PL emission was dispersed with a grating and collected with an InGaAs array detector.

The low temperature PL spectra of the GaSb QWs and QD ensembles were measured at 20 K in a closed-loop He-cooled cryostat. The samples were excited with a 532 nm laser with a broad excitation spot having a diameter of 1.3 mm FWHM. The PL emission was collected and focused with lenses towards a 0.5 m monochromator and then detected with an InGaAs photodiode. Standard lock-in technique with thermoelectric cooling of the detector was used for improving the signal-to-noise ratio.

Single-QD emission was studied by micro-PL at 6 K using a low-vibration closed-loop He-cooled cryostat. Individual QDs were excited non-resonantly with a 965 nm laser diode through a confocal lens ($f=2.75$ mm, $NA=0.68$) and a 2 mm diameter hemispherical solid immersion lens. The PL emission from the QD was collected with the same lenses, dispersed with a 750 mm spectrograph, and detected with thermoelectric-cooled InGaAs array.

ASSOCIATED CONTENT

Supporting Information. Surface morphology below critical Al coverage; Surface morphology of filled nanoholes; Illustration of the MBE-grown layer structures

AUTHOR INFORMATION

Corresponding Author

*teemu.hakkarainen@tuni.fi

Author Contributions

The manuscript was written through contributions of all authors. All authors have given approval to the final version of the manuscript.

Funding Sources

Academy of Finland Project QuantSi (decision No. 323989)

Academy of Finland Project NanoLight (decision No. 310985)

ACKNOWLEDGMENT

The authors acknowledge financial support from the Academy of Finland Projects QuantSi (decision No. 323989) and NanoLight (decision No. 310985)

REFERENCES

1. Arakawa, Y.; Holmes, M. J. Progress in quantum-dot single photon sources for quantum information technologies: A broad spectrum overview. *Applied Physics Reviews* **2020**, *7*, 021309. DOI:10.1063/5.0010193
2. Lee, J.; Leong, V.; Kalashnikov, D.; Dai, J.; Gandhi, A.; Krivitsky, L. A. Integrated single photon emitters. *AVS Quantum Science* **2020**, *2*, 031701. DOI:10.1116/5.0011316
3. Madhukar, A.; Xie, Q.; Chen, P.; Konkar, A. Nature of strained InAs three-dimensional island formation and distribution on GaAs (100). *Appl. Phys. Lett.* **1994**, *64*, 2727-2729. DOI:10.1063/1.111456
4. Moison, J.; Houzay, F.; Barthe, F.; Leprince, L.; Andre, E.; Vatel, O. Self-organized growth of regular nanometer-scale InAs dots on GaAs. *Appl. Phys. Lett.* **1994**, *64*, 196-198. DOI:10.1063/1.111502
5. Sanguinetti, S.; Bietti, S.; Koguchi, N. *Droplet epitaxy of nanostructures; Molecular Beam Epitaxy - From Research to Mass Rroduction, 2nd Edition*; Henini, M., Ed.; Elsevier: 2018; pp 293-314
6. Kuroda, T.; Mano, T.; Ha, N.; Nakajima, H.; Kumano, H.; Urbaszek, B.; Jo, M.; Abbarchi, M.; Sakuma, Y.; Sakoda, K. Symmetric quantum dots as efficient sources of highly entangled photons: Violation of Bell's inequality without spectral and temporal filtering. *Physical Review B* **2013**, *88*, 041306. DOI:10.1103/PhysRevB.88.041306

7. Gurioli, M.; Wang, Z.; Rastelli, A.; Kuroda, T.; Sanguinetti, S. Droplet epitaxy of semiconductor nanostructures for quantum photonic devices. *Nature materials* **2019**, *1*. DOI:10.1038/s41563-019-0355-y
8. Felici, M.; Gallo, P.; Mohan, A.; Dwir, B.; Rudra, A.; Kapon, E. Site-Controlled InGaAs Quantum Dots with Tunable Emission Energy. *Small* **2009**, *5*, 938-943. DOI:10.1002/sml.200801274
9. Versteegh, M. A.; Reimer, M. E.; Jöns, K. D.; Dalacu, D.; Poole, P. J.; Gulinatti, A.; Giudice, A.; Zwiller, V. Observation of strongly entangled photon pairs from a nanowire quantum dot. *Nature communications* **2014**, *5*, 1-6. DOI:10.1038/ncomms6298
10. Heyn, C.; Stemmann, A.; Köppen, T.; Strelow, C.; Kipp, T.; Grave, M.; Mendach, S.; Hansen, W. Highly uniform and strain-free GaAs quantum dots fabricated by filling of self-assembled nanoholes. *Appl. Phys. Lett.* **2009**, *94*, 183113. DOI:10.1063/1.3133338
11. Atkinson, P.; Zallo, E.; Schmidt, O. Independent wavelength and density control of uniform GaAs/AlGaAs quantum dots grown by infilling self-assembled nanoholes. *J. Appl. Phys.* **2012**, *112*, 054303. DOI:10.1063/1.4748183
12. Keil, R.; Zopf, M.; Chen, Y.; Höfer, B.; Zhang, J.; Ding, F.; Schmidt, O. G. Solid-state ensemble of highly entangled photon sources at rubidium atomic transitions. *Nature communications* **2017**, *8*, 1-8. DOI:10.1038/ncomms15501
13. Liu, J.; Su, R.; Wei, Y.; Yao, B.; da Silva, Saimon Filipe Covre; Yu, Y.; Iles-Smith, J.; Srinivasan, K.; Rastelli, A.; Li, J. A solid-state source of strongly entangled photon pairs with high brightness and indistinguishability. *Nature nanotechnology* **2019**, *14*, 586-593. DOI:10.1038/s41565-019-0435-9
14. Huo, Y.; Rastelli, A.; Schmidt, O. Ultra-small excitonic fine structure splitting in highly symmetric quantum dots on GaAs (001) substrate. *Appl. Phys. Lett.* **2013**, *102*, 152105. DOI:10.1063/1.4802088
15. Huber, D.; Reindl, M.; Huo, Y.; Huang, H.; Wildmann, J. S.; Schmidt, O. G.; Rastelli, A.; Trotta, R. Highly indistinguishable and strongly entangled photons from symmetric GaAs quantum dots. *Nature communications* **2017**, *8*, 1-7. DOI:10.1038/ncomms15506
16. Schöll, E.; Hanschke, L.; Schweickert, L.; Zeuner, K. D.; Reindl, M.; Covre da Silva, Saimon Filipe; Lettner, T.; Trotta, R.; Finley, J. J.; Müller, K. Resonance fluorescence of GaAs quantum dots with near-unity photon indistinguishability. *Nano letters* **2019**, *19*, 2404-2410. DOI:10.1021/acs.nanolett.8b05132
17. Stemmann, A.; Heyn, C.; Köppen, T.; Kipp, T.; Hansen, W. Local droplet etching of nanoholes and rings on GaAs and AlGaAs surfaces. *Appl. Phys. Lett.* **2008**, *93*, 123108. DOI:10.1063/1.2981517

18. Lee, J. H.; Wang, Z. M.; Ware, M. E.; Wijesundara, K. C.; Garrido, M.; Stinaff, E. A.; Salamo, G. J. Super low density InGaAs semiconductor ring-shaped nanostructures. *Crystal Growth and Design* **2008**, *8*, 1945-1951. DOI:10.1021/cg701263c
19. Li, A. Z.; Wang, Z. M.; Wu, J.; Xie, Y.; Sablon, K. A.; Salamo, G. J. Evolution of holed nanostructures on GaAs (001). *Crystal Growth and Design* **2009**, *9*, 2941-2943. DOI:10.1021/cg900189t
20. Stemmann, A.; Köppen, T.; Grave, M.; Wildfang, S.; Mendach, S.; Hansen, W.; Heyn, C. Local etching of nanoholes and quantum rings with In_xGa_{1-x} droplets. *J. Appl. Phys.* **2009**, *106*, 064315. DOI:10.1063/1.3225759
21. Wang, Z. M.; Liang, B.; Sablon, K.; Salamo, G. Nanoholes fabricated by self-assembled gallium nanodroplet on GaAs (100). *Appl. Phys. Lett.* **2007**, *90*, 113120. DOI:10.1063/1.2713745
22. Alonso-González, P.; Fuster, D.; González, L.; Martín-Sánchez, J.; González, Y. Low density InAs quantum dots with control in energy emission and top surface location. *Appl. Phys. Lett.* **2008**, *93*, 183106. DOI:10.1063/1.3021070
23. Heyn, C.; Stemmann, A.; Hansen, W. Dynamics of self-assembled droplet etching. *Appl. Phys. Lett.* **2009**, *95*, 173110. DOI:10.1063/1.3254216
24. Heyn, C.; Stemmann, A.; Hansen, W. Nanohole formation on AlGaAs surfaces by local droplet etching with gallium. *J. Cryst. Growth* **2009**, *311*, 1839-1842. DOI:10.1016/j.jcrysgro.2008.11.001
25. Hilska, J.; Chellu, A.; Hakkarainen, T. Diffusion-driven nanohole etching in AlGaSb with Ga droplets. *arXiv preprint arXiv:2101.09106* **2021** DOI:arXiv:2101.09106
26. Gisin, N.; Thew, R. Quantum communication. *Nature photonics* **2007**, *1*, 165-171. DOI:10.1038/nphoton.2007.22
27. Vurgaftman, I.; Meyer, J. á; Ram-Mohan, L. á Band parameters for III-V compound semiconductors and their alloys. *J. Appl. Phys.* **2001**, *89*, 5815-5875. DOI:doi.org/10.1063/1.1368156
28. Wang, J.; Sciarrino, F.; Laing, A.; Thompson, M. G. Integrated photonic quantum technologies. *Nature Photonics* **2020**, *14*, 273-284. DOI:10.1038/s41566-019-0532-1
29. Ferrini, R.; Patrini, M.; Franchi, S. Optical functions from 0.02 to 6 eV of Al_xGa_{1-x}Sb/GaSb epitaxial layers. *J. Appl. Phys.* **1998**, *84*, 4517-4524. DOI:10.1063/1.368677
30. Huang, S.; Balakrishnan, G.; Khoshakhlagh, A.; Jallipalli, A.; Dawson, L.; Huffaker, D. Strain relief by periodic misfit arrays for low defect density GaSb on GaAs. *Appl. Phys. Lett.* **2006**, *88*, 131911. DOI:10.1063/1.2172742

31. Huang, S.; Balakrishnan, G.; Khoshakhlagh, A.; Dawson, L.; Huffaker, D. Simultaneous interfacial misfit array formation and antiphase domain suppression on miscut silicon substrate. *Appl. Phys. Lett.* **2008**, *93*, 071102. DOI:10.1063/1.2970997
32. Rodriguez, J.; Madiomanana, K.; Cerutti, L.; Castellano, A.; Tournié, E. X-ray diffraction study of GaSb grown by molecular beam epitaxy on silicon substrates. *J. Cryst. Growth* **2016**, *439*, 33-39. DOI:10.1016/j.jcrysgro.2016.01.005
33. Lu, Q.; Zhuang, Q.; Marshall, A.; Kesaria, M.; Beanland, R.; Krier, A. InSb quantum dots for the mid-infrared spectral range grown on GaAs substrates using metamorphic InAs buffer layers. *Semiconductor Science and Technology* **2014**, *29*, 075011. DOI:10.1088/0268-1242/29/7/075011
34. Glaser, E.; Bennett, B.; Shanabrook, B.; Magno, R. Photoluminescence studies of self-assembled InSb, GaSb, and AlSb quantum dot heterostructures. *Appl. Phys. Lett.* **1996**, *68*, 3614-3616. DOI:10.1063/1.115747
35. Deguffroy, N.; Tasco, V.; Baranov, A.; Tournié, E.; Satpati, B.; Trampert, A.; Dunaevskii, M.; Titkov, A.; Ramonda, M. Molecular-beam epitaxy of InSb/GaSb quantum dots. *J. Appl. Phys.* **2007**, *101*, 124309. DOI:<https://doi.org/10.1063/1.2748872>
36. Küster, A.; Heyn, C.; Ungeheuer, A.; Juska, G.; Moroni, S. T.; Pelucchi, E.; Hansen, W. Droplet etching of deep nanoholes for filling with self-aligned complex quantum structures. *Nanoscale research letters* **2016**, *11*, 1-7. DOI:10.1186/s11671-016-1495-5
37. Heyn, C.; Schnüll, S.; Hansen, W. Scaling of the structural characteristics of nanoholes created by local droplet etching. *J. Appl. Phys.* **2014**, *115*, 024309. DOI:10.1063/1.4861722
38. Miyata, N.; Ohtake, A.; Ichikawa, M.; Mori, T.; Yasuda, T. Electrical characteristics and thermal stability of HfO₂ metal-oxide-semiconductor capacitors fabricated on clean reconstructed GaSb surfaces. *Appl. Phys. Lett.* **2014**, *104*, 232104. DOI:10.1063/1.4882643
39. Cebulla, U.; Forchel, A.; Tränkle, G.; Griffiths, G.; Subbanna, S.; Kroemer, H. Direct-indirect band gap crossover in two-dimensional GaSb/AlSb-quantum-well-structures. *Superlattices and microstructures* **1987**, *3*, 429-434. DOI:10.1016/0749-6036(87)90218-7
Get rights and content
40. Farfad, S.; Leon, R.; Leonard, D.; Merz, J.; Petroff, P. Phonons and radiative recombination in self-assembled quantum dots. *Physical Review B* **1995**, *52*, 5752. DOI:10.1103/PhysRevB.52.5752
41. Ulhaq, A.; Duan, Q.; Zallo, E.; Ding, F.; Schmidt, O. G.; Tartakovskii, A.; Skolnick, M.; Chekhovich, E. A. Vanishing electron g factor and long-lived nuclear spin polarization in weakly strained nanohole-filled GaAs/AlGaAs quantum dots. *Physical Review B* **2016**, *93*, 165306. DOI:10.1103/PhysRevB.93.165306

42. Tonomura, S.; Yamaguchi, K. Uniform formation of high-density InAs quantum dots by InGaAs capping growth. *J. Appl. Phys.* **2008**, *104*, 054909. DOI:10.1063/1.2975366
43. Klenovský, P.; Steindl, P.; Geffroy, D. Excitonic structure and pumping power dependent emission blue-shift of type-II quantum dots. *Scientific reports* **2017**, *7*, 1-10. DOI:10.1038/srep45568
44. Weiß, M.; Krenner, H. J. Interfacing quantum emitters with propagating surface acoustic waves. *J. Phys. D* **2018**, *51*, 373001. DOI:10.1088/1361-6463/aace3c